Journal of Aerosol Science 166 (2022) 106063

Contents lists available at ScienceDirect

Journal of Aerosol Science

journal homepage: www.elsevier.com/locate/jaerosci

Tutorial: Dynamic organic growth modeling with a volatility basis set

Dominik Stolzenburg [a,*], Mingyi Wang [b,c], Meredith Schervish [b,d], Neil M. Donahue [b]

[a] Institute for Atmospheric and Earth System Research/Physics, University of Helsinki, 00014, Helsinki, Finland
[b] Center for Atmospheric Particle Studies, Carnegie Mellon University, Pittsburgh, 15217, PA, USA
[c] Division of Chemistry and Chemical Engineering, California Institute of Technology, Pasadena, 91125, CA, USA
[d] Department of Chemistry, University of California, Irvine, Irvine, CA, 92697, USA

ARTICLE INFO

Keywords:
aerosol Dynamics
Organic aerosols
Nanoparticle growth
Volatility basis set

ABSTRACT

Organic aerosols are ubiquitous in the atmosphere and oxygenated organics are a major driver of aerosol growth. The volatility basis set (VBS) as introduced by Donahue et al. (2006, 2011) is often used to simplify the partitioning behavior of the huge variety of atmospheric organics. Recently, the VBS was used to dynamically model aerosol growth from the smallest sizes onwards. This tutorial is intended to equip the reader with the necessary tools to facilitate organic growth modelling based on gas-phase measurements of oxygenated organics using a 2-dimensional VBS. We start with a contextualization of the VBS in partitioning theory and point out the need for dynamic modeling. We provide an overview on the most common methods to estimate the volatility of oxygenated organics and give detailed instruction on how to construct the binned VBS. We then explain the dynamic condensation model including solution and curvature effects. Furthermore, we provide a python package for VBS growth calculations and show with two examples from ambient and chamber measurements how growth rates can be calculated. Last, we summarize the limitation of this approach and outline necessary future developments.

1. Introduction

Organic aerosols are an important constituent of the atmosphere and organic species dominate the submicron aerosol mass at many locations around the world (Spracklen et al., 2011). They are either directly emitted primary organic particles or secondary organic aerosols (SOA) formed in the atmosphere when the oxidation products of organic vapors form a particulate phase via nucleation, condensation or multiphase chemistry (Hallquist et al., 2009; Jimenez et al., 2009). However, the effects of SOA on the Earth's radiative balance or its impact on human health are not fully quantified (Daellenbach et al., 2020; IPCC, 2021), as models still have difficulties in reproducing measured SOA abundances and show significant discrepancies among each other (Spracklen et al., 2011; Tsigaridis et al., 2014). On the one hand, this is because SOA forms from oxidation of a wide variety of volatile organic compounds (VOCs) of both natural and anthropogenic origins, with a wide range of possible oxidation processes producing hundreds of thousands of different organic constituents in the atmosphere (Goldstein & Galbally, 2007). On the other hand, the frequently reported underestimation of SOA in large-scale models could be due to incomplete theoretical description of SOA condensation. Many models are based on SOA mass formation experiments where the organic compounds are condensed onto pre-existing seed particles and the

* Corresponding author.
E-mail address: dominik.stolzenburg@helsinki.fi (D. Stolzenburg).

https://doi.org/10.1016/j.jaerosci.2022.106063
Received 27 April 2022; Received in revised form 22 July 2022; Accepted 24 July 2022
Available online 28 August 2022
0021-8502/© 2022 The Authors. Published by Elsevier Ltd. This is an open access article under the CC BY license (http://creativecommons.org/licenses/by/4.0/).

quantity of interest is the yield of aerosol mass per reacted precursor (Hallquist et al., 2009). These yields are often used within absorptive partitioning theory (Donahue et al., 2006; Odum et al., 1996; Pankow, 1994b) to distribute the produced organic mass onto the aerosol size-distribution assuming instantaneous equilibration between the gas- and particle-phase for organic compounds, meaning that new SOA mass is distributed evenly across the organic aerosol mass distribution (or whatever portion of the mass distribution the SOA is assumed to partition into). However, recent experiments showed that highly oxygenated organic molecules (HOMs) can also form new particles and efficiently grow them from the smallest sizes onwards (Kirkby et al., 2016). In that case of new particle formation (NPF) and growth the mass transfer to the particle phase becomes a dynamic process due to the extremely low saturation vapor pressure and low abundances of these compounds in atmospherically relevant settings (Ehn et al., 2014; Tröstl et al., 2016). This is especially important in the growth of particles formed by atmospheric NPF, where HOMs might be the key drivers (Bianchi et al., 2016; Kulmala et al., 2013; Pierce et al., 2011; Tröstl et al., 2016). As NPF is a major contributor to the global cloud condensation nuclei budget (Gordon et al., 2017), a dynamic modelling approach for new particle growth is preferred to better describe the organic condensation behavior (Riipinen et al., 2011; Xi Zhang et al., 2012). Additionally, such approaches can take into account dynamic losses to chamber walls in experiments, which might be a reason for underpredicted SOA budget when smog chamber experiments are used as input for large-scale models (La et al., 2016; Xuan Zhang et al., 2014).

The volatility basis set (VBS) was developed to model the evolution of organic aerosol in the atmosphere (Donahue, Epstein, Pandis, & Robinson, 2011; Donahue et al., 2006). It is used to facilitate organic aerosol partitioning considerations by lumping together organic compounds with similar volatility into so-called volatility bins thereby reducing the overwhelming variety of abundant atmospheric organic constituents (Goldstein & Galbally, 2007) along the volatility axis. However, recent refinements have adapted the VBS concept to the dynamic condensation of organics (D. Stolzenburg et al., 2018; Tröstl et al., 2016). Besides laboratory experiments, the VBS was also used to describe the initial growth of aerosol particles in the boreal forest (Mohr et al., 2019). Chuang and Donahue (2017) point out that there are crucial differences between the partitioning approach and the dynamic modelling of the condensation process. Here, we intend to describe the approach of modelling dynamic condensation with a VBS in full detail such that the reader is equipped with the necessary basics to perform such calculations. We will also provide two examples and discuss possible limitations of the approach. Altogether, this tutorial should provide the basis for correct future applications and improvements of the VBS approach to dynamic growth modelling.

2. Methods

2.1. Organic partitioning theory

We start with classical partitioning theory of an organic compound i with a saturation mass concentration of c_i^0 expressed in μg m^{-3}. Note that saturation mass concentration is used as the equivalent of saturation vapor pressure p_i^0 (or saturation number concentration $N_{i,eq}$) here and the transformation between them is given via the ideal gas law in Eq. (1):

$$c_i^0 = \frac{p_i^0 M_i}{k_B T} = N_{i,eq} M_i \tag{1}$$

where M_i is the molecular mass (in g) of the organic species. Note that these relations are also often expressed using the molecular weight (g mol^{-1}) and the gas constant R and the equilibrium molarity $n_{i,eq}$ (in mol m^{-3}). Absorptive partitioning theory developed by Pankow (1994a, 1994b) defines a relation between the mass concentration found in the gas and particle-phase, $c_{i,g}$ and $c_{i,p}$ respectively. It is convenient to use the form given by Donahue et al. (2006) using the total particulate organic mass c_{OA}, the fraction of i found in the particle phase, i.e. $F_i = c_{i,p}/(c_{i,p} + c_{i,g}) = c_{i,p}/c_{i,t}$ and the saturation mass concentration c_i^* as shown in Eq. (2):

$$F_i = \left(1 + \frac{c_i^*}{c_{OA}}\right)^{-1} \tag{2}$$

This equation couples the total particulate organic mass $c_{OA} = \sum_i F_i \cdot c_{i,t}$ to the mass fraction in the particle phase of an individual compound F_i and needs to be solved iteratively for c_{OA}. Here, the effective saturation mass concentration $c_i^* = \gamma_i c_i^0$ is used, which takes into account the non-ideality of the solution of i in the total absorbing organic phase described by the mass based activity coefficient γ_i (Donahue, Epstein, et al., 2011; Donahue et al., 2006). It is defined such that Raoult's law describing the vapor pressure above a solution of i is expressed in terms of mass fraction $\varphi_i = c_{i,p}/c_{OA}$, i.e. $p_i = \varphi_i \gamma_i p_i^0$. Other formulations using a molar activity coefficient ζ_i exist (Pankow, 1994a) defining Raoult's law on the molar fraction $\chi_i = n_{i,p}/n_{i,t}$, i.e. $p_i = \chi_i \zeta_i p_i^0$. Note that, the mass and molar based activity coefficients are not equal but can be related through the ratio of the molar weight of solute and solvent. However, the underlying concept remains the same and Donahue et al. (2006, 2011) argues that the usage of mass based activity coefficient for similar density organics is well justified. In that case, the mass based approach describes the physical exclusion of material from the surface which is the basis of Raoult's law, with the advantage that mass based formulation is often easier to access experimentally via bulk atomic composition and aerosol mass measurements. There is an apparent relation between the particulate mass fraction of the compound i and the total organic mass given by Eq. (2) that increasing the total organic mass c_{OA} will drive the compound i into the particle phase. Note that the total organic mass c_{OA} is not strictly defined as the organic fraction of the total suspended particles, but as the absorptive phase (Pankow, 1994a). This may well include water or inorganics, as long as the compound i is absorbed in that phase (Donahue et al., 2006). The relation between F_i, c_i^* and c_{OA} is typically illustrated by the fact that if $c_i^* = c_{OA}$, 50% of compound i will be

found in the particle phase and 50% in the gas phase. However, the equilibrium analysis is contingent on equilibrium actually being appropriate, which is, especially in atmospheric aerosol growth, where vapour production and losses are dynamic, very often not the case (Chuang & Donahue, 2017).

2.2. Mass transfer within dynamic condensation

If we approach the problem of organic mass transfer from the gas- to the particle-phase from a dynamic perspective we start with the differential equations for mass transfer expressed for an individual compound i to a monodisperse particle population with N_p particles (Seinfeld & Pandis, 2016):

$$\frac{dc_{i,p}}{dt} = N_p k_{i,p}\left(c_{i,g} - a_{i,p}c_i^0\right) \tag{3}$$

Here, $k_{i,p}$ is the collision rate coefficient of compound i with these particles (expressed in $cm^3\ s^{-1}$, such that multiplied with the concentration of particles and vapor the number of collisions per unit volume and unit time are obtained). Accounting for the size of both the vapor and particle (Nieminen et al., 2010), we use the coagulation coefficient assuming spherical particles and vapors as given by Fuchs & Sutugin (1971) including the mass accommodation coefficient $\alpha_{i,p}$ for vapor i on particle p and correcting for the effects of the transition regime via the correction factor $\beta_{i,p}$:

$$k_{i,p} = 2\pi\left(d_i + d_p\right)\left(D_i + D_p\right)\cdot\beta_{i,p} \text{ with } \beta_{i,p} = \frac{(1+Kn)}{1 + \left(0.377 + \frac{4}{3\alpha_{i,p}}\right)Kn + \frac{4}{3\alpha_{i,p}}Kn^2} \tag{4}$$

where $d_{i/p}$ and $D_{i/p}$ are the vapor/particle diameters and diffusion coefficients, respectively. We adjust the Knudsen number to $Kn = \frac{2\lambda}{d_i+d_p}$ with the mean free path (mean persistence distance between vapor and particle) $\lambda = 3(D_i+D_p)(\bar{c}_i^{\,2} + \bar{c}_p^{\,2})^{-\frac{1}{2}}$ for the non-negligible effect of vapor-molecular size (Lehtinen & Kulmala, 2003; Nieminen et al., 2010), where $D_{i/p} = k_B T C_C(d_{i/p})/3\pi\eta d_{i/p}$ is the diffusion coefficient of vapor or particle with the Cunningham slip correction $C_C(d_{i/p}) = 1.0 + Kn(1.165 + 0.483\cdot\exp(-0.997/Kn))$ and $\bar{c}_{i/p} = \sqrt{8RT/\pi d_{i/p}}$ is the mean thermal velocity. The Knudsen number defined that way still indicates the collision regime of interest for the collision between the vapor and the particle, with $Kn \to \infty$ as the kinetic and $Kn \to 0$ as the continuum regime.

The last term of Eq. (3), $(c_{i,g} - a_{i,p}c_i^0)$ is the so-called driving force of condensation. It can also be expressed as a function of the saturation mass concentration and the difference between the gas- and particle phase activity of the substance resulting in the modified mass transfer equation:

$$\frac{dc_{i,p}}{dt} = N_p k_{i,p} c_i^0\left(S_i - a_{i,p}\right) \tag{5}$$

here $S_i = c_{i,g}/c_i^0$ is the saturation ratio, i.e. the gas-phase activity defined as the ratio of actual gas-phase mass concentration of the compound $c_{i,g} = \frac{p_i M_i}{k_B T} = N_i M_i$ (in analogy to Eq. (1)) and the saturation mass concentration itself. The term $a_{i,p} = K_i \cdot \frac{c_{i,p}}{c_{OA}}\gamma_i$ is the particle-phase activity; this is subject to the Raoult term to account for the reduced vapor pressure of the individual compounds in the organic mixture including the activity coefficient $\frac{c_{i,p}}{c_{OA}}\gamma_i$; and a Kelvin term $K_i = \exp\left(\frac{4\sigma_{OA}M_i}{RT\rho_{OA}d_p}\right)$, which in turn accounts for the increased equilibrium vapor pressure over curved surfaces and can be estimated using (bulk) organic surface tension σ_{OA}, density ρ_{OA} and the molecular mass M_i of the condensing compound. As these underlying parameters are often not well constrained, the Kelvin effect is also expressed via a Kelvin-diameter $d_k = \log(e)\cdot\frac{4\sigma_{OA}M_i}{RT\rho_{OA}}$ such that $K_i = 10^{d_k/d_p}$ and hence d_k becomes the characteristic particle size, where the increased equilibrium vapor pressure due to particle curvature becomes relevant (Donahue, Trump, Pierce, & Riipinen, 201; D. Stolzenburg et al., 2018; Tröstl et al., 2016).

2.3. The volatility basis set

So far we only have considered one condensing compound, however the complexity of atmospheric organic aerosol goes far beyond thousands of different molecules which can participate in growth (Goldstein & Galbally, 2007). Donahue et al. (2006) proposed grouping this variety of compounds into bins according to their volatility (saturation mass concentration), as this is the quantity which defines the partitioning. While the focus in partitioning theory was mainly put on semi-volatile organics which are the more abundant oxygenated organic molecules (OOMs), more recent research identified the crucial role of compounds which extremely favor the particle-phase and have very low vapor pressures. These volatility bins are separated by powers of 10 in saturation mass concentration and we classify them ranging from ultra low-volatility compounds (ULVOC, $c_i^* \leq 10^{-9}$ μg m^{-3}, the "nucleator" compounds, Simon et al., 2020), extremely low-volatility compounds (ELVOC, $c_i^* = 10^{-8}\ldots10^{-5}$ μg m^{-3}) and low-volatility compounds (LVOC, $c_i^* = 10^{-4}\ldots0.1$ μg m^{-3}) up to semi-volatile organic compounds (SVOC, $c_i^* = 1\ldots100$ μg m^{-3}) or intermediate volatility organic compounds (IVOC, $c_i^* = 10^3\ldots10^6$ μg m^{-3}). Depending on temperature and ambient organic aerosol levels, c_{OA}, these species can either reside in the gas- or particle phase. Assuming equilibrium conditions the ELVOC clearly prefer the particle-phase and IVOC prefer the gas-phase under almost all circumstances. This also implies that for most practical applications where only gas-to-particle conversion is of interest, we can crop the VBS by summing up all bins smaller than a certain volatility and adding them to the least volatile bin which will

reside in the particle-phase and, in turn, we can omit all bins larger than a certain volatility as they will anyways reside in the gas-phase. This typically limits the VBS to a set of 8–12 volatility bins, the fixed basis set of volatility. We will illustrate this reasoning of the VBS by describing smog chamber SOA formation as it was done by Presto & Donahue (2006) in the following example.

2.3.1. *Example: VBS inferred from smog chamber SOA formation experiments*

Smog chamber experiments typically oxidize a certain amount of precursor VOC and measure the aerosol mass formed per unit of precursor, the so-called aerosol mass fraction $AMF = \frac{\Delta c_{OA}}{\Delta VOC}$ (often also called SOA yield). However, the formed particulate aerosol mass depends on the total organic aerosol loading of the experiment and hence on the amount of oxidized precursor as we have seen above in Eq. (2). Therefore, we expect to measure a different AMF for different amounts of total VOC reacted. Fig. 1 shows results from various smog chamber experiments of α-pinene ozonolysis at low NO_x levels as presented in Presto & Donahue (2006). In a 10-m^3 teflon chamber, at ozone levels of several hundreds of ppb, α-pinene was injected from tens to hundreds of ppb and the subsequent aerosol mass formation was monitored with a scanning mobility particle sizer and the AMF was calculated assuming an aerosol density of 1 g cm^{-3} and correcting for aerosol wall losses. The AMF is shown in dependence of the total organic aerosol loading c_{OA} as introduced first by Odum et al. (1996). The portioning behavior of a certain VOC is often described by a 2-product model assuming $VOC \rightarrow \alpha_1 P_1(c_1^*) + \alpha_2 P_2(c_2^*)$ with the volatility $c_{1,2}^*$, and total product (gas- plus particle phase mass) yields $\alpha_{1,2}$ of these surrogate products as the free parameters (Odum et al., 1996). The two products can be understood as lumped species describing the ensemble of all low-volatility (P_1) and semi-volatile (P_2) reaction products. If we assume that the oxidation chemistry remains the same independent of the aerosol loading c_{OA} (which might be very much not the case), then the mass yield of each (real) reaction product should be constant, i.e. $VOC \rightarrow \alpha_1 P_1 + \alpha_2 P_2 + \ldots + \alpha_m P_m$. As each product is assigned to the same VBS bin independent of the total aerosol loading, this also means that the mass yields of the n VBS bins α_i remain constant across different loadings c_{OA}. Therefore, as the volatility of all bins is already defined, the AMF versus c_{OA} dependence can be described only using the yields α_i as free parameters in the VBS approach by coupling the reaction equation to Eq. (2), as shown in Eq. (6):

$$AMF = \sum_{i=1}^{n} \alpha_i \cdot F_i = \sum_{i=1}^{n} \alpha_i \cdot \left(1 + \frac{c_i^*}{c_{OA}}\right)^{-1} \tag{6}$$

This removes the high correlation of $\alpha_{1,2}$ and $c_{1,2}^*$ in the 2-product fit, which often resulted in ambiguities when adding new data to the fit inducing large changes of the estimated parameters which makes it very difficult to compare different 2-product fit results with each other (Presto & Donahue, 2006). The VBS is a nearly orthogonal set of parameters, as there is little cross-talk between neighboring bins if they are spaced with one order of magnitude in volatility. At a given $c_{OA} = c_i^*$, bin i is semi-volatile with a 50/50 partitioning, but already c_{i-1}^* and c_{i+1}^* have either 90% of the material in the particle or gas-phase, respectively. This also makes the fitting of the basis set

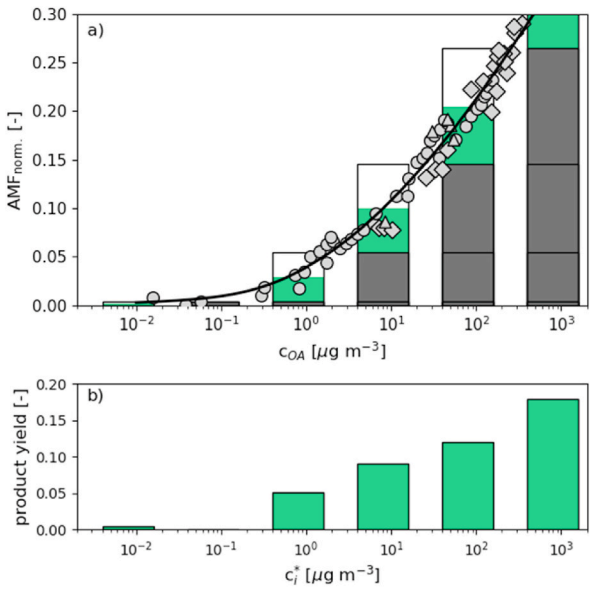

Fig. 1. VBS inferred from smog chamber experiments following the reasoning of Presto & Donahue (2006). (a) shows the aerosol mass fraction (AMF or SOA Yield) in dependence of the total aerosol loading c_{OA} for α-pinene ozonolysis SOA formation experiments conducted by different groups (grey symbols, data from Presto & Donahue, 2006 and references therein). The black line is the fitted VBS according to Eq. (6) and the gray bars indicate the fully condensed material from the bins with $c_i^* < c_{OA}/10$. The light green bars represent the semi-volatile bin at a specific c_{OA} where 50/50 partitioning occurs. (b) shows the VBS distribution as inferred from (a). It can be subsequently used to predict partitioning under dilution, temperature change or chemical ageing (Donahue et al., 2006). (For interpretation of the references to color in this figure legend, the reader is referred to the Web version of this article.)

to the smog chamber data very illustrative. If we neglect the 10% cross-talk entirely, and start from AMF results at low-c_{OA}, where at $c_{OA} \sim 0.01$ μg m^{-3} the total mass yield is roughly 0.002 and is contributed entirely by the $c^*_{i=0} = 0.01$ μg m^{-3} bin portioning in a 50/50 behavior which indicates a product yield $\alpha_{i=0} = 0.004$. For the next bin, we can then assume that $c^*_{i=0}$ is entirely condensed but as no difference in mass yield is observed we infer a zero product yield in the $c^*_{i=1} = 0.1$ μg m^{-3} bin. This procedure is repeated, i.e. in the third bin we assume that $c^*_{i<2}$ is condensed and as the rest of the observed AMF at this total aerosol loading c_{OA} is assumed to be contributed from the 50/50 partitioning of $c^*_{i=2} = 1$ μg m^{-3} bin. That way, we can intuitively understand the fit result shown in Fig. 1a and infer the VBS distribution shown in Fig. 1b. The advantage of the VBS approach is then that once the VBS for a certain precursor is obtained, different conditions such as dilution, mixing, temperature changes can be described within the same formalism allowing predictions of the partitioning behavior in chemical transport models (Donahue et al., 2006, 2009; Lane et al., 2008). However, while this approach is straight forward, it is contingent on the key assumptions that the SOA system in the experiment is in equilibrium and also that wall losses of vapors are minimal or at least constant.

2.4. 2d-VBS: organic volatility and O:C

Chuang and Donahue (2016) and Donahue et al. (2011, 2012) developed a 2-dimensional VBS by extending the volatility axis with the degree of oxygenation as the second dimension to better describe oxidation chemistry, solution thermodynamics and mixing. Measurements of bulk aerosol average oxidation state ($\overline{OS_c}$ or as an alternative the oxygen to carbon ratio, O:C) with the aerosol mass spectrometer (Aiken et al., 2008) are nowadays widely available and can be used to constrain this second dimension of the 2d-VBS. The most important concept of the 2d-VBS remains that the volatility (c^*) is the important quantity needed to understanding partitioning, regardless of whether a molecule is identified or not, and that the bulk composition of the solvent (O:C) is often measured. It can be discretized, as implied by "basis set" and this is conventionally into bins separated by factors of 10 in c^* (discretization along the O:C dimension is typically not applied). However, individual molecules with known composition can be located in the space exactly, while the likely composition (n_C, n_O, etc.) can be estimated.

The usage of the average O:C to define the interaction behavior of organic aerosol is based on the reasoning that the great complexity of the organic mixture can be reduced to interactions of functional groups. Pankow & Asher (2008) showed that there are distinct relations between different functional groups of organic compounds and their pure component vapor pressures. This is illustrated in Fig. 2a, where the experimentally derived pure component saturation mass concentrations for several molecules are plotted versus their carbon number for classes of molecules with different functionalization. It can be seen that across all classes, vapor pressure scales with the number of carbon atoms with roughly half a decade in saturation mass concentration per n_c and that acids lower the vapor pressure more significantly than alcohols or carbonyls (i.e. ketones and aldehydes). However, for the 2d-VBS space it is the effect per oxygen atom which is important (as we are interested in O:C), where the effect on volatility alters between 1 decade per oxygen (carbonyls, i.e. ketones and aldehydes) to 1.75 decades per oxygen (acids) and 2.3 decades per oxygen (alcohols), which, due to the same underlying dataset, is consistent with the group-contribution method (Pankow & Asher, 2008). Donahue, Epstein, et al. (2011) assumed that, on average, these main functional groups of organic aerosol exist in roughly constant and equal relative fractions. This results in an effective decrease by 1.7 decades in volatility per oxygen atom constraining a simple parametrization of pure-component saturation mass concentration according to their oxygen and carbon number:

$$\log_{10} c_i^0 = \left(n_C^0 - n_C\right) b_C - n_O b_O \text{ with } n_c^0 = 25,\ b_c = 0.475,\ b_O = 1.7 \tag{7}$$

As we can see in Fig. 2a, Eq. (7) results in a prediction in between the carbonyls and alcohols for the addition of one oxygen atom, but the available data were heavily biased towards high vapor pressures and low O:C ratios. An offset is already apparent for the diacids, which explains the need for the introduction of a non-linearity term in the parametrization (Donahue, Epstein, et al., 2011):

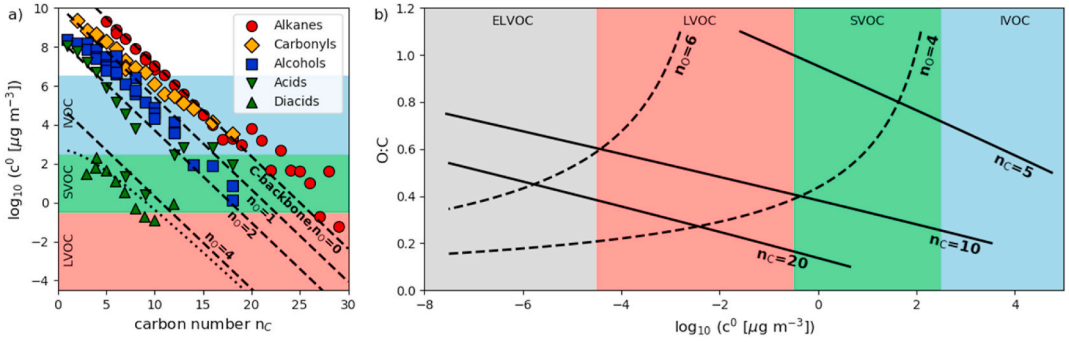

Fig. 2. 2d-VBS with O:C as second dimension. (a) shows the relation between carbon number and pure component saturation mass concentration for molecules with different functionalization indicated by different symbols, data from Donahue, Epstein, et al. (2011). Black dashed lines show the volatility – O:C relation according to Eq. (8) for 0, 1, 2 and 4 oxygen atoms. Black dotted line shows the volatility – O:C relation according to Eq. (8). (b) shows the 2D-VBS and the relation between carbon and oxygen number by indicating isopleths of 5, 10 and 20 carbon atoms and 4 and 6 oxygen atoms.

$$\log_{10} c_i^0 = \left(n_C^0 - n_C\right) b_C - n_O b_O - 2\frac{n_C n_O}{n_C + n_O} b_{CO} \text{ with } n_c^0 = 25, b_c = 0.475, b_O = 2.3, b_{CO} = -0.3 \quad (8)$$

Note the adjustment of the oxygen effect b_O in order to obtain the correct limit at low O:C, i.e. Eq. (7). That way, the 2d-VBS was designed to provide average composition information (the average carbon, oxygen and hydrogen numbers n_C, n_O and n_H, respectively) of the OA due to experimentally constrained O:C and vapor pressures, i.e. the position of organic aerosol fraction in the 2d-VBS space, which is illustrated in Fig. 2b with the isopleth lines for different numbers of carbon and oxygen atoms. However, as we will see below, modern mass spectrometry has made individual compound identification accessible across a wide range of organic volatilities and oxidation states, especially for the more limited amount of species which could potentially participate in NPF and early growth. Therefore, the argument of the 2d-VBS can also be turned around: If we can constrain the composition of the OOMs, we can predict their behavior along the bulk properties of the same O:C and volatility as found in the 2d-VBS. However, this additionally requires adjustments to the O:C volatility relation to account for more complex functionality in organic aerosol.

2.5. Volatility parametrizations for complex organic mixtures

While the initial parametrization of the 2d-VBS by Donahue, Epstein, et al. (2011) neglected the effect of nitrogen and other functionality than alcohols, carbonyls and acids, oxygenation of organics in the atmosphere often proceeds via autoxidation (Bianchi et al., 2019; Ehn et al., 2014) and in the presence of NO_x, which favors functionalization into hydroperoxides, peroxyacids (Bianchi et al., 2019) and nitrate groups (Yan et al., 2020; Zhao et al., 2018). Contributions from such groups are however not accounted in the average oxygen contribution to volatility as laid out in the initial 2d-VBS (Donahue, Epstein, et al., 2011) and require adjustment to the volatility parametrization of Eq. (8). For biogenic autoxidation products under no-NO_x conditions, Tröstl et al. (2016) showed that the volatility-O:C relation needs an adjustment in the case of α-pinene ozonolysis products as the OOMs originating from autoxidation will contain a significant amount of hydroperoxides. They proposed a simple fit of the volatility inferred via the group-contribution method of Pankow & Asher (2008) for some theoretically proposed molecular structures. Stolzenburg et al. (2018) refined the simple fit of by using the same form as Eq. (8) but with an adjusted effect of oxygen on volatility showing that the effect on volatility per oxygen atom is reduced when the abundant hydroperoxides are included in the relation:

$$\log_{10} c_i^0 = \left(n_C^0 - n_C\right) b_C - n_O b_{O,adj.} - 2\frac{n_C n_O}{n_C + n_O} b_{CO} \text{with } n_c^0 = 25, b_c = 0.475, b_O = b_{O,mon./dim.}, b_{CO} = -0.3 \quad (9)$$

The adjusted effect of oxygen $b_{O,adj.}$ was separately determined for monomer and covalently bound dimers, because the latter also include peroxide bounds, even further lowering the effect on volatility per oxygen with $b_{O,mon.} = 1.4$ and $b_{O,dim.} = 1.17$. The validity of Eq. (9) for the α-pinene ozonolysis system was confirmed for a wide range of temperatures (see Sect. 2.6 for the temperature effect) by direct measurements of the volatility of the condensed phase products via thermal desorption mass spectrometry and mass balance in particle growth (D. Stolzenburg et al., 2018; Wang et al., 2020; Ye et al., 2019). However, Eq. (9) is derived for zero NO_x conditions, and in most ambient setting NO_x interferes with the oxidation chemistry of organics, especially also in autoxidation (Yan et al., 2020). Assuming that nitrogen is incorporated into organic aerosols mostly via nitrate groups, Pankow & Asher (2008) suggest an effect of 2.5 decades in volatility per nitrate group, however, we now need to take into account that 3 oxygen molecules of n_O cannot contribute to different functionalization. In that sense the parametrization by Stolzenburg et al. (2018) and Donahue, Epstein, et al. (2011) can be adjusted:

$$\log_{10} c^0 = \left(n_C^0 - n_C\right) b_C - (n_O - 3n_N) b_O - 2\frac{n_C(n_O - 3n_N)}{n_C + n_O - 3n_N} b_{CO} - n_N b_N \quad (10)$$

with all parameters as above but b_O and b_{CO} depending on the chosen parametrization summarized in Table 1. This effect of nitrogen is also incorporated into the parametrization of Mohr et al. (2019) which was successfully applied to a dataset from the boreal forest showing mass balance between the gas-phase products and the observed particle growth with $b_O = 0.2$, $b_{CO} = 0.9$, which results in a weakened effect of oxygen with increasing O:C giving the limit of Eq. (8) for low O:C and approaching Eq. (9) for high O:C, indicating that the hydroperoxides start to contribute more significantly for more advanced autoxidation. However, when directly measuring the volatility via thermal desorption is seems that also at low O:C the volatility of biogenic oxidation products undergoing autoxidation is clearly distinct from multi-generation oxidation products from anthropogenic precursors (Wang et al., 2020). Ultimately, it is case specific which volatility parametrization of Table 1 needs to be applied when the VBS is inferred from direct product measurements and it can be especially challenging when the organic mixture is highly complex including both multi-generation oxidation products and organics originating from autoxidation.

Table 1
Parameters used in the volatility parametrization of Eq. (10) used by different authors. Note that, the parametrization by Stolzenburg et al. (2018) differentiates between monomers ($n_C \leq 10$) and dimers ($n_C > 11$) from α-pinene autoxidation.

Parametrization	n_C^0	b_C	b_O	b_{CO}	b_N
Donahue, Epstein, et al. (2011)	25	0.475	2.3	−0.3	2.5
Stolzenburg et al. (2018)	25	0.475	Monomer: 1.4, Dimer: 1.17	−0.3	2.5
Mohr et al. (2019)	25	0.475	0.2	0.9	2.5

This challenge may be resolved by identifying the precursors of individual OOMs, and then using the corresponding VBS parameterizations accordingly. However, it is likely that the traditional source apportionment methods such as the positive matrix factorization do not provide sufficient resolving power as the temporal variation in OOMs may well be driven by the variation of atmospheric oxidants or condensation sink; additional criteria based on existing knowledge of VOC oxidation are thus required. For example, Nie et al. (2022) developed a workflow to assign OOMs measured in four Chinese megacities into four groups (aliphatic-OOMs, aromatic-OOMs, isoprene-OOMs and monoterpene-OOMs), according to their distinct molecular properties, such as the number of carbon atoms (n_C), effective oxygen atoms (n_{O-eff}) nitrogen atoms (n_N), and the double bond equivalent (DBE $= (2n_C + 2 - n_H - n_N)/2$). They then adopt the parameterizations used in Mohr et al. (2019) and Donahue, Epstein, et al. (2011) to estimate the volatility of the monoterpene-OOMs and other types of OOMs, respectively, and yielded a reasonably good closure in OOM condensation flux.

2.5.1. Example: VBS inferred from direct product measurements

Atmospheric pressure interface chemical ionization mass spectrometry has made the measurement and quantification of individual gas-phase organic molecules at the sub-pptv level available (Breitenlechner et al., 2017; Ehn et al., 2014; Riva et al., 2019). Therefore, atmospheric organic oxidation products can be measured directly in the gas-phase, even if their vapor pressures are so low that most of them will condense. The mass-resolving power of time-of-flight mass spectrometers allows for the precise identification of the molecular composition of many of these OOMs. If the carbon and oxygen number of a compound are identified, Eq. (10) can thus be used to estimate the product specific vapor pressure of individual compounds. However, these estimates are averages assuming the average share of functionalization among carbonyls, acids and alcohols (or hydroperoxides in the presence of autoxidation) and by no means representative for an individual molecule. Therefore, we group the molecules into the bins of the 1D-VBS arguing that the variation of the vapor pressure of individual molecules due to different functionalization averages at least across one bin. Fig. 3a shows a mass defect plot for product identification of toluene oxidation products measured with iodide-adduct chemical ionization (Lee et al., 2014) in a well-controlled chamber experiment (Wang et al., 2020). Mass defect (actual mass minus integer mass based on ^{12}C) plots help to clearly identify series of molecules with similar chemical composition, in that case the increase in oxygen number is manifested in a series towards the lower right while the increase in carbon number is manifested by a step towards the upper right. Once the molecular composition is identified, Eq. (10) is applied (using Donahue, Epstein, et al., 2011 parametrization see Table 1) to assign each peak a volatility at 300 K and the VBS bins are filled accordingly as shown in Table 2 (example of the LVOC peaks not containing nitrogen). The bins are separated by one order of magnitude in volatility as explained above, spanning from e.g. $\log_{10} c^*$ in [−4.5,-5.5) or $c^{*\text{in}}$ [$3.16{\cdot}10^{-5}$ µg m^{-3},$3.16{\cdot}10^{-6}$ µg m^{-3}), with the higher volatility bound closed and the lower volatility bound open. Peaks are assigned to one bin only and no fractional assignment of their concentration according to their calculated $\log_{10} c_i^*$ is performed, as the latter approach does not improve the VBS distribution as the overall uncertainty in volatility estimates is at least one order of magnitude in c^*. We keep track of the concentration weighted average mass of each bin, while the nominal volatility is per definition set to the c_i^* of the bin.

2.5.2. Example: direct volatility measurements with thermal desorption methods

As we have seen above, several parametrizations for the 2d-VBS O:C volatility space exits due to different considerations on the possible structures and functionalization (D. Stolzenburg et al., 2018; Tröstl et al., 2016). However, the underlying group contribution methods were inferred from datasets at rather low O:C and higher volatilities. It is therefore preferred to obtain volatility measurements of individual compounds for the volatility range of interest in organic growth, i.e. the ELVOC, LVOC and low SVOC range. One method is thermal desorption measurements, where aerosol particles are collected via filters or electrostatic deposition and subsequently heated, vaporized and analyzed in chemical ionization mass spectrometers (CIMS), where the peak temperature of the

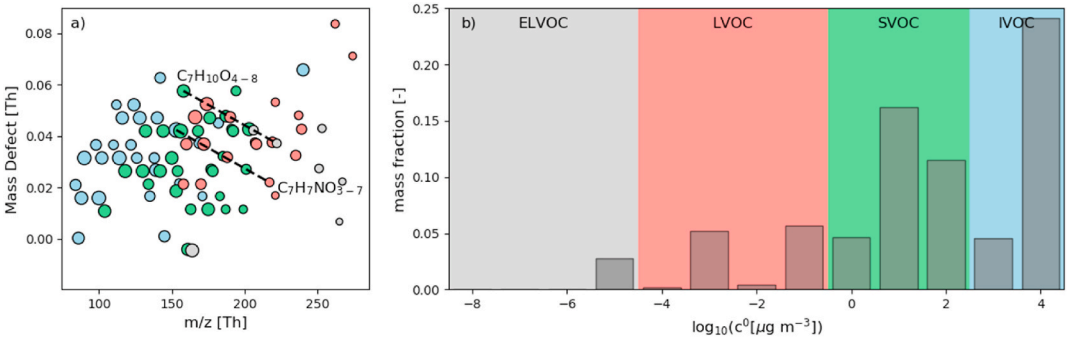

Fig. 3. VBS inferred from direct gas-phase product measurements for a toluene oxidation experiment (Wang et al., 2020). (a) shows a mass defect plot of the oxidation products measured by iodide-adduct chemical ionization (monomer range) with the color-code indicating the volatility class assigned at 300 K (light blue IVOC, light green SVOC, coral LVOC and grey ELVOC) and the size is proportional to the logarithm of the signal. Dashes lines show series of different products, the $C_7H_8O_{5-9}$ and $C_7H_{10}O_{4-8}$ series. (b) shows the resulting VBS distribution (normalized to the total oxidized organic signal as measured by iodide-adduct chemical ionization) at 300 K. (For interpretation of the references to color in this figure legend, the reader is referred to the Web version of this article.)

Table 2
Conversion of the molecular identified signal for ELVOC peaks of toluene oxidation experiments into the corresponding VBS bins. After molecular identification (sum formula) Eq. (11) and the parametrization of Donahue, Epstein, et al. (2011) are used to infer the volatility $\log_{10} c_i^0$ at 300 K of each compound, which results in the bin assignment. For further calculations we keep track of the number of molecules in each bin and the concentration weighted average mass. The concentration weighted average volatility is not further used, as within the VBS, the bins get assigned their midpoint volatility. In this example case we use the relative concentration of each molecule to the total signal assuming equal detection efficiency for all OOMs.

sum formula	Mass [amu]	rel. concentration	$\log_{10}(c_i^0$ [$\mu g\ m^{-3}$])	assigned bin
$C_4H_4O_7$	163.996	0.027422	−4.56	[-4.5,-5.5)
$C_7H_{10}O_7$	206.043	0.000639	−5.45	[-4.5,-5.5)
$C_7H_{10}O_8$	222.038	0.000339	−7.61	[-7.5,-8.5)
$C_7H_9NO_9$	251.028	0.000285	−5.81	[-5.5,-6.5)
$C_7H_{11}NO_9$	253.043	0.000217	−5.81	[-5.5,-6.5)
$C_7H_7NO_{10}$	265.007	0.000071	−7.95	[-7.5,-8.5)
$C_7H_9NO_{10}$	267.023	0.000103	−7.95	[-7.5,-8.5)
bin [$\log_{10} c_i^*$]	nbr. of molecules	conc. av. mass	av. conc	av. $\log_{10}(c_i^*$ [$\mu g\ m^{-3}$])
−5	2	164.954	0.028061	−4.62
−6	2	252.898	0.000502	−5.81
−7	0			
−8	3	237.026	0.000513	−7.73

desorption signal of an individual compound can be connected to its vapor pressure. Fig. 4a shows the calibration of such direct volatility measurements for two sets of calibration data of a filter inlet for gas and aerosols (FIGAERO) coupled to CIMS (Lopez-Hilfiker et al., 2014). Ylisirniö et al. (2021) pointed out that there are significant discrepancies between these different calibrations which can cause huge deviations in the inferred VBS distribution. The authors linked these discrepancies to the calibration method and concluded that calibration substances should be atomized and deposited as aerosol particles on the FIGAERO to simulate a realistic desorption behavior. Moreover, literature based reference saturation vapor pressures for the calibration compounds also suffer from uncertainties (especially for the often used organic acids), which are as large as one order of magnitude and thus the usage of a homologous series of polyethylene glycols is suggested (Krieger et al., 2018; Ylisirniö et al., 2021). If such thorough calibration procedures are applied, the desorption temperature, i.e. the temperature with the maximum signal of an individual desorbed compound, can be correlated with its vapor pressure. This allows for a direct determination of the compound in the 2d-VBS space, but it needs to be noted that fragmentation or pyrolysis effects during the heating can still systematically disturb the volatility prediction of gas-phase constituents by this particle-phase based approach. Nevertheless, Fig. 4b and c shows reasonable agreement between FIGAERO based volatility estimates and the parameterizations of Table 1 are depicted in the same panel. Especially lower volatility compounds with high molecular weight (dimers, Fig. 4c) seem to be very well predicted by the thermal desorption method. There is more spread among the monomers for both aromatic and biogenic precursors, which could be due to dehydration and fragmentation effects during the thermal desorption (Wang

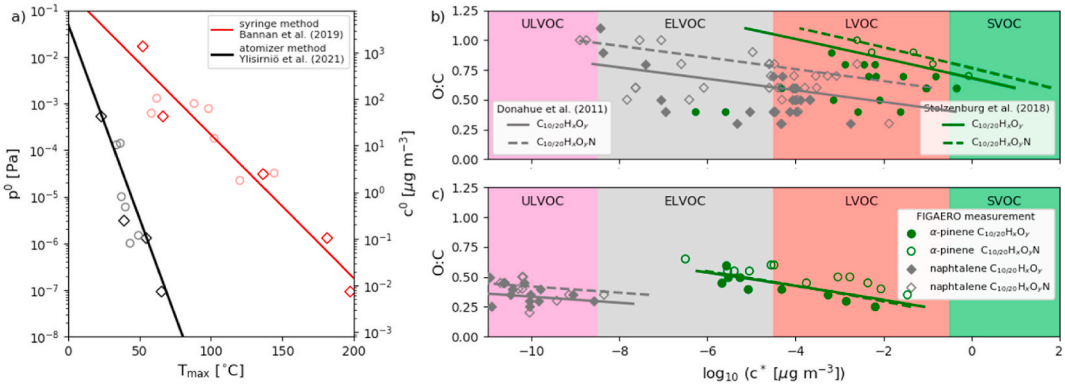

Fig. 4. The usage of direct volatility measurements using thermal desorption of a FIGAERO-CIMS. (a) shows the comparison of two different calibration methods with the syringe method (Bannan et al., 2019) in red and the atomizer method (Ylisirniö et al., 2021) in black. Different organic acids (light circles) and a homologous series of polyethylene glycols were used in both methods, with the latter preferred due to the reduced uncertainties in reference vapor pressure. (b) and (c) show the O:C volatility relation for compounds measured with the FIGAERO method, with the green symbols representing α-pinene oxidation products and the gray symbols representing naphthalene oxidation products (open for compounds including a nitrate group and filled symbols without nitrogen for both systems). The solid and dashed lines show the corresponding volatility parametrizations from Table 1, with green following Stolzenburg et al. (2018) and gray following Donahue, Epstein, et al. (2011), dashed lines including one nitrogen, solid lines without nitrogen. (b) shows the monomers (C_{10} compounds) and (c) the dimers (C_{20} compounds), where for the latter a different b_O is used in the Stolzenburg et al. (2018) parametrization. (For interpretation of the references to color in this figure legend, the reader is referred to the Web version of this article.)

et al., 2020).

2.6. Temperature dependence

As we have seen in Section 2.4.1 the bins are always filled at 300 K, as the original definition of the VBS including its 2d-parametrization were defined at that temperature and follow the underlying trends of organics as shown in Fig. 2a, which were observed at 300K. The temperature dependence can be treated on the VBS scale (Donahue et al., 2006) and the saturation mass concentration shifts according to the approximated Clausius-Claperyon equation expressed in terms of saturation mass concentration (Epstein et al., 2010) as follows:

$$\log_{10} c^0(T) = \log_{10} c^0(300K) + \frac{1000 \cdot \Delta H_{vap}}{R \cdot \ln(10)} \left(\frac{1}{300} - \frac{1}{T} \right) \tag{11}$$

We see that the temperature dependence scales with the enthalpy of vaporization ΔH_{vap} (as the entropy of vaporization is nearly constant over liquids and other disordered materials). ΔH_{vap} can then be linked to the volatility at 300 K by an empirical linear fit as demonstrated by Epstein et al. (2010), which is a solid approximation for near room temperature systems:

$$\Delta H_{vap} \left[\frac{\text{kJ}}{\text{mol K}} \right] = a \cdot \log_{10} c^0(300K) + b \tag{12}$$

We typically assume that ΔH_{vap} is constant over the smaller temperature ranges usually needed in most ambient considerations of mass transfer but a treatment of $\Delta H_{vap}(T, c^0)$-dependence is presented in Epstein et al. (2010). For the simple approximation, again different parametrizations exist with $a = -5.7$, $b = 100$ (Donahue, Epstein, et al., 2011), $a = -11$, $b = 129$ (Epstein et al., 2010). Stolzenburg et al. (2018) used a hybrid of both with $a = -5.7$, $b = 129$ which resulted in a better agreement for the observed mass balance in nanoparticle growth at cold temperatures and which was subsequently used by Simon et al. (2020) and Ye et al. (2019). The three different volatility-enthalpy of vaporization relations are illustrated in Fig. 5a. It is important to note that the most significant differences due to these parametrizations occur at very low vapour pressures (nominal, i.e. at 300K), where the bins will mostly anyways reside in the particle phase. For temperatures close to 300 K (i.e. most ambient settings at mid-latitudes and low altitudes) the temperature effect on growth is most important for the bins in the LVOC and SVOC range (at 300K), where the differences between the different parametrizations are small (Fig. 5a and b). Fig. 5c shows the effect of a temperature shift over a large temperature range. The VBS is filled at 300 K, even if the particles collected and analysed with the FIGAERO-CIMS were produced at −50 °C (223 K). While the particle-phase compounds would mostly be semi-volatile at 300 K, they are ranging from the ULVOC to LVOC range at that low

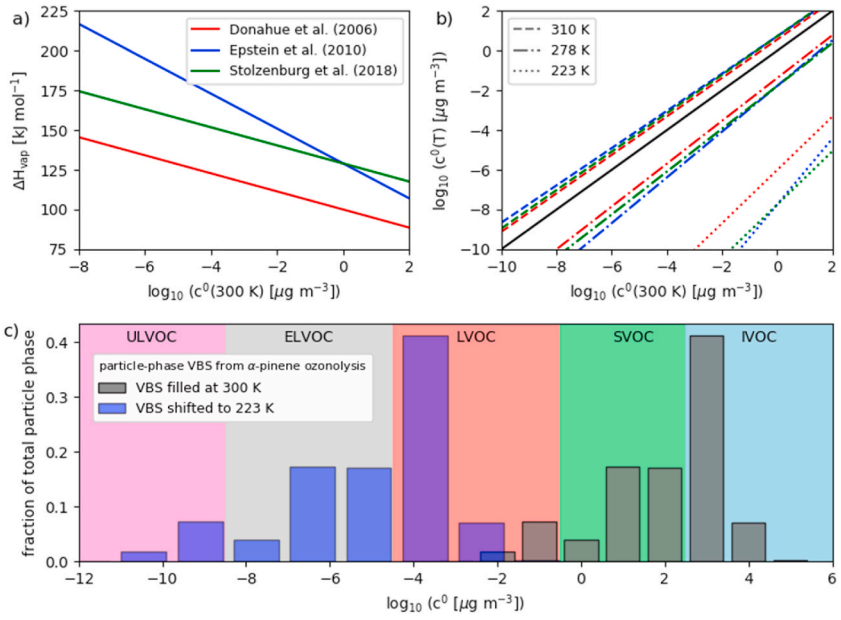

Fig. 5. Temperature dependence of volatility and the corresponding VBS. (a) shows three different relations between the enthalpy of vaporization ΔH_{vap} and the volatility $\log c^0(300\,K)$ and (b) shows the shift in volatility for temperature changes from 300 K to 310 K (37 °C), 278 K (5 °C) and down to 223 K (−50 °C), demonstrating that the deviations between the different temperature approaches become most significant at very low temperatures (well below the typical mid-latitude and low altitude range) or at very low volatility (where the products are anyways residing in the particle phase). (c) shows the volatility distribution of particle phase measurements with a FIGAERO-CIMS during an α-pinene ozonolysis experiment at −50 °C. The gray bars show the VBS filled at 300 K and the blue bars show the shifted VBS the actual temperature of the experiment. (For interpretation of the references to color in this figure legend, the reader is referred to the Web version of this article.)

temperature. Note that the VBS distribution has not changed between 300 and 223 K, only the bins have been shifted and broadened (they would shrink at T > 300 K) but no individual compounds have changed their bin. The latter is the important characteristic of the VBS.

2.7. Coupled dynamic condensation equations for nucleation mode growth

So far we have discussed how to setup the 2d-VBS at different temperatures and for different chemical systems based on the direct measurements of gas- or particle-phase composition with high resolution tools, often also providing information on the volatility of these compounds. We have also illustrated the underlying principles originating from partitioning theory, but now we will use the 2d-VBS to dynamically model the mass transfer for aerosol growth within a monodisperse (or as we will see equivalently, single-particle) growth model.

If we aim to describe nucleation mode growth, we can reduce the computational load by cropping the 2d-VBS to a set of 8–12 bins, spanning from $\log_{10} c_i^* = 2\ldots0$ down to $\log_{10} c_i^* = -6\ldots-10$. As explained above, the measured concentrations are summed up for all compounds below the lowest volatility of a given set of VBS-bins, are assigned to the lowest bin and are used in the concentration average of the mean molecular mass of that bin (as they will all still contribute to growth); likewise, for all bins above the highest volatility we omit the compounds (as they will never reside in the particle phase under conditions typical for nucleation mode growth). We are then faced with a set of 8–12 coupled differential equations for the bins i of the VBS as described by Eq. (3) and shown in its full form (specifying Kelvin and Raoult effect) below:

$$\frac{dc_{i,p}}{dt} = N_p k_{i,p} c_i^0 \left(\frac{c_{i,g}}{c_i^0} - \gamma_i \frac{c_{i,p}}{c_{OA}} \cdot \exp\left(\frac{4\sigma_{OA} M_i}{RT\rho_{OA} d_p} \right) \right) \text{ with } c_{OA} = \sum_i c_{i,p} \tag{13}$$

Here N_p is the number concentration of the monodisperse growing mode with diameter d_p, which is dynamically evolving as it is linked to the total particle phase organic mass concentration c_{OA} and total number concentration:

$$d_p = \left(\frac{6 c_{OA}}{\pi \rho_{OA} N_p} \right)^{1/3} \tag{14}$$

Here ρ_{OA} is the density of the organics and σ_{OA} is the surface tension, which are both assumed to be equal across all VBS bins, while for the molecular mass M_i we typically can use the concentration averaged property as described above. $k_{i,p}(d_i, d_p)$ is the collision rate coefficient of the molecules of bin i with the particles of size d_p, as defined by Eq. (4). However, it is important to note that the collisions responsible for nucleation mode growth are almost entirely in the kinetic regime ($Kn \to \infty$), and hence the diffusion limitation in the collision rate coefficient is very minor. Hence, it is better to express the collision kernel with the transition regime correction factor multiplied to the kinetic collision rate, where it becomes apparent that the diffusivity only enters the expression via the transition regime correction $\gamma = \frac{4}{3} Kn\, \beta_{i,p}$:

$$k_{i,p}(d_i, d_p) = \frac{\pi}{4} (d_i + d_p)^2 \left(\bar{c}_i^2 + \bar{c}_p^2 \right)^{1/2} \cdot \frac{4}{3} Kn\, \beta_{i,p} \text{ with } \beta_{i,p} \text{ as above} \tag{15}$$

The collision kernel could also include interaction potentials, which is straight-forward to add to the free molecular collision rate coefficient via an enhancement factor:

$$k'_{i,p}(d_i, d_p) = \frac{\pi}{4} (d_i + d_p)^2 \left(\bar{c}_i^2 + \bar{c}_p^2 \right)^{1/2} \cdot \eta_{FM} \tag{16}$$

Including the transition regime with interaction potentials (resulting intermolecular forces, e.g. van-der-Waals forces or electrostatic force) is more challenging and we generally refer to the various definitions for the enhancement factor, which can be found in e.g. Ouyang et al. (2012) or Stolzenburg et al. (2020). However, while we assume all vapor molecules and particles to be uncharged, van-der-Waals forces due to dipoles are currently not well-quantified for OOMs and hence the collision enhancement is neglected in the following, but is optional in our vbsgrowth python package.

Using that collision kernel we can rearrange the terms in Eq. (13) and obtain a different formulation of the mass transfer equation as used e.g. in Tröstl et al. (2016) or Chuang and Donahue (2017):

$$\frac{dc_{i,p}}{dt} = N_p \cdot \underbrace{\frac{\pi}{4} (d_p + d_i)^2}_{\substack{\text{particle-vapor} \\ \text{collision cross-section}}} \cdot \overbrace{\alpha_{i,p} \nu_{i,p} \beta'_{i,p}}^{\substack{\text{deposition rate of} \\ \text{vapors at the surface}}} \cdot \underbrace{\left(c_{i,g} - a_{i,p} c_i^0 \right)}_{\substack{\text{driving force of} \\ \text{condensation}}} \tag{17}$$

where $\beta'_{i,p} = \frac{4}{3\alpha_{i,p}} Kn \cdot \beta_{i,p}$ is the adjusted Fuchs & Sutugin correction factor and $\nu_{i,p} = \left(\bar{c}_i^2 + \bar{c}_p^2 \right)^{1/2} = \sqrt{8RT/\pi\mu_{i,p}}$ is the center of mass velocity of the colliding entities with the reduced mass $\mu_{i,p} = m_i m_p / (m_i + m_p)$. While both formulations (Eq. (13) and Eq. (17)) are equivalent, the latter shows the separation of the geometric collision cross-section and deposition rate of the vapor at the surface, which includes the kinetics of the collision and the gas-phase gradients near the particle and connected to it, the accommodation coefficient.

We see that the 8–12 equations for all VBS bins following Eq. (13) (or equivalently Eq. (17)) are coupled through the total particulate organic mass concentration c_{OA} and the activity coefficients, which are a function of the particle-phase chemical composition $\gamma_i(c^*_{i,p})$. However, once the initial values of $c_{i,p}(t_0)$ are known and $c_{i,g}(t)$ is obtained from measurements or a gas-phase chemistry box model (and the functions $\gamma_i(c^*_{p,i})$ are known), we end up with an initial value problem of coupled differential equations, which can be solved numerically. Typically Eulerian forward methods can be used and to avoid numerical instabilities we suggest the usage of solvers for stiff problems, which are provided e.g. by both MATLAB and python.

3. Results and discussion

3.1. Algorithm description

We are interested in the diameter growth rate of the particle $GR = dd_p/dt$, i.e. the $d_p(t)$ trajectory of a monodisperse particle population. The monodispersity simplification might induce problems as it omits second order diffusion-driven growth (Olenius et al., 2018) and future work needs to explore that. The integration of Eq. (13) will track the organic particle phase mass concentrations $c_{i,p}(t)$ which are linked to the diameter as seen in Eq. (14). As mentioned above we treat all other variables as input or calculate them along the trajectory of the solution.

Step 1. *Define the initial value problem.*

In order to define the problem we need to set the initial values $c_{i,p}(t_0)$. We start with particles of diameter $d_p = 0.9$ nm, i.e. as close as possible to the size of a critical cluster for nucleation, which are present in a number concentration of $N_p = 1000\ \mathrm{cm}^3$, but we will see later that in some specific cases the absolute value of N_p does not influence the results of the $d_p(t)$ trajectory. We assume that this initial particulate mass $c_{OA}(t_0) = c_{seed}$ of the seed is non-volatile and doesn't change during the simulation ($\frac{dc_{seed}}{dt} = 0$), and hence $c_{OA}(t) = c_{OA}(t_0) \cdot \gamma_{seed} + c_{VBS}(t)$ with $c_{VBS} = \sum_i c_{i,p}$ as defined before and we include an interaction term for the seed material γ_{seed} (equivalent to an activity coefficient in the sense that it describes the extent of phase-separation between seed and condensing organics, but not the evaporation behavior according to Raoult's law due to the non-volatile assumption). This interaction term, if set to 0, would result in a behavior where the VBS organics are essentially insoluble in the seed and if set to 1, the VBS organics entirely dissolve in the seed and it need to be taken into account in the total particulate organic mass $c_{OA}(t)$ during the simulation. The activity coefficients $\gamma_i(c^*_{p,i})$ are set 1 in this version of the algorithm, following the reasoning of Donahue, Epstein, et al. (2011) and Tröstl et al. (2016) that the condensing organics are similar enough in O:C and $\log c^*$ (i.e. in their location in the 2d-VBS) that they should have close-to-unity activity coefficients for the typical particle-phase compositions of the growing nucleation mode aerosol. A description of the $\gamma_i(c^*_{p,i})$-functions could be incorporated in future versions of the algorithm.

Other input variables can be defined by the user. The values $\rho_{OA} = 1400\ \mathrm{kg\ m^{-3}}$ and $\sigma_{OA} = 0.03\ \mathrm{N\ m^{-1}}$ were found to correctly predict the Kelvin term in organic growth with a Kelvin-diameter $d_k = 4.8$ nm at 300 K (D. Stolzenburg et al., 2018). The molecular mass M_i and gas-phase mass concentration $c_{i,g}$ are taken from the input VBS of the specific problem to be solved. We can use a time-independent $c_{i,g}$ assuming constant production and sink rates, or use measured $c_{i,g}(t)$ values assuming steady-state between gas- and particle-phase at the measurement time t. Note that, $c_{i,g}(t)$ often requires the conversion from measured number-based concentration to saturation mass concentration, equivalently to Eq. (1). Last, it is also possible to model the production and losses of the gas-phase VBS bins and dynamically infer their concentrations, however, in this case the simulation becomes dependent on the particle sink defined through the growing monodisperse population, i.e. the choice of N_p is not arbitrary anymore if the particle growth rate remains the quantity of interest. We refer to Tröstl et al. (2016) or Chuang and Donahue (2017) for such cases, with the latter also extending the approach to a polydisperse particle population. Here, our aim is to recover the nucleation mode growth rate and not reproduce smog chamber experiments and therefore we focus on the cases where $c_{i,g}$ is time-independent or directly measured.

Step 2. *Solve the $d_p(t)$ trajectory and VBS-bin mass fluxes.*

We need to set up the 8–12 differential equations according to Eq. (13) and also define 8–12 differential equations for the gas-phase assuming a linear behavior between two consecutive measurements of the gas-phase VBS at t_{n+1} and t_n with

$$\frac{dc_{i,g}}{dt} = \frac{c_{i,g}(t_{n+1}) - c_{i,g}(t_n)}{t_{n+1} - t_n} \tag{18}$$

as the differential equation solution is typically calculated in finer time-steps than measurements are available. If the gas-phase VBS is taken from a dynamic chemistry model, its evolution could be incorporated at that stage. We implement a function which describes the gradients, i.e. the left hand sides of Eqs. (13) and (18) and use that function together with the initial values as input for the ordinary differential equation solver. For an solver-internal integration time-step of Δt (typically below 1 min) we can calculate the forward Eulerian solution $c_{i,p}(t)$ and $c_{i,g}(t)$ until a maximum time t_{end}, which is either defined by the end of the observations of the gas-phase VBS $c_{i,g}(t)$ or by a certain diameter $d_{p,\max}$ reached on the growth trajectory, defined by Eq. (14).

We are additionally interested in the mass flux per VBS bin, and we use the solution $c_{i,p}(t)$ to transform it to a diameter growth rate attributed to each VBS bin $\frac{dd_{i,p}}{dt}(t)$:

$$\frac{dc_{i,p}}{dt}(t) = \frac{d\left(\rho_{OA}\frac{\pi}{6}d_{i,p}^3 N_p\right)}{dt}(t) = \rho_{OA}\frac{\pi}{6}N_p 3d_{i,p}^2\frac{dd_{i,p}}{dt}(t) \tag{19}$$

This can be equated with Eq. (13) and we see that $\frac{dd_{i,p}}{dt}(t)$ is then independent of the monodisperse particle population N_p demonstrating that its choice is indeed arbitrary. The total growth rate caused by the specific VBS distribution can then be calculated as the sum of all individual contributions. To estimate the uncertainty of the growth rate calculation we suggest to shift the entire VBS distribution by one order of magnitude in volatility at 300 K in both directions (which corresponds to the above discussed uncertainty in volatility assignment) and calculate the corresponding growth trajectories.

We implemented the VBS growth dynamic calculation within the python module vbsgrowth available at https://version.helsinki.fi/atm-public/vbsgrowth. The package provides functionality to calculate volatility from measured oxygen, carbon and nitrogen numbers, calculation of collision kinetics and the ordinary differential equation solver for the coupled equations following Eq. (13). We describe the module alongside two example datasets from a well-controlled chamber experiment and ambient measurements.

3.2. CLOUD experiment

Our first example case is mass spectrometric input data from the CERN CLOUD experiment (Kirkby et al., 2011), where we use an example case of constant vapor concentrations over the run, as the main loss mechanism is the wall loss rate resulting in a steady-state vapor concentration dominated by the balance of wall loss and gas-phase production via α-pinene ozonlysis. In contrast to the smog chamber experiments presented above, α-pinene levels were more than one order of magnitude lower and the condensable vapor losses to the walls become a significant dynamic factor (Chuang & Donahue, 2017), whereas in the smog chamber experiments the ratio of condensation sink and wall losses was dominated by the former. While smog chamber experiments aimed at matching the produced total particulate organic mass with partitioning theory, CLOUD studies the nucleation and growth and hence it is essentially the saturation ratios of the organic ensemble which needs to be predicted correctly. The used experiments at 5 °C are similar to Stolzenburg et al. (2018), where two different ionization techniques have been applied to cover the broad range of OOMs produced in the chamber: nitrate-chemical ionization at ambient pressure (nitrate-CI; Jokinen et al., 2012) and proton-transfer-reaction ionization at reduced pressure with a novel inlet (PTR3; Breitenlechner et al., 2017). For details on the peak identification and quantification of both methods we refer to the two aforementioned publications and Stolzenburg et al. (2018).

When combining data from two mass spectrometers, we need to assume that the molecular ion signals detected at the same masses (subject to subtraction of the reagent ion) correspond to the same oxidation product, neglecting different isomers and hydrogen abstraction or fragmentation during the ionization process in either of the two devices. Even if both instruments should be capable of performing quantitative gas-phase measurements for specific compounds, the detection (mainly ionization) efficiency for the full range of OOMs is not known for either of the two utilized ionization techniques. Dedicated laboratory experiments have shown that different ionization chemistries have a different sensitivity to different degrees of oxygenation for OOMs (Riva et al., 2019). After loading the mass spectrometric data we therefore combine the two instruments by using only the stronger signal for peaks identified in both instruments. We apply the Stolzenburg et al. (2018) parametrization (Table 1) in order to assign each peak a saturation mass concentration c^0 and for simplicity set $c^* = c^0$, i.e. $\gamma = 1$ for all identified molecules. As discussed in Donahue, Epstein, et al. (2011) for a two component case, the similar location of all peaks in the 2d-VBS space might justify the assumption of unity activity coefficients. We

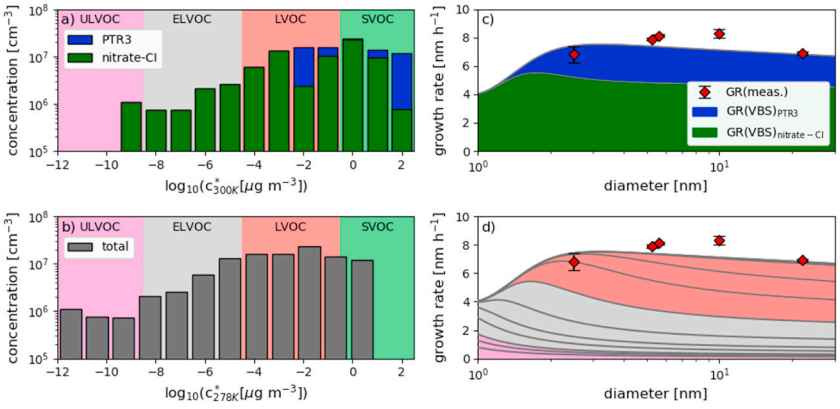

Fig. 6. Example results from a dataset of the CERN CLOUD chamber using two different ionization techniques. (a) and (b) show the VBS distribution as obtained from the gas-phase measurements of OOMs. (a) at 300 K, where the VBS is filled and resolved for the contributions of the nitrate-CI (green bars) and PTR3 (blue bars), such that the total bar height represents the total measured concentration in each bin. (b) at 278 K the temperature of the experiments. (c) and (d) show the resulting modelled growth curve (growth rate versus diameter). (c) resolved for the contributions measured by the nitrate-CI (green) and PTR3 (blue). (d) resolved in the contributions of the individual VBS-bins, with the color-code indicating their rough volatility range at 278 K, plum ULVOC, gray ELVOC, coral LVOC, the light-green SVOC contribution on top of the LVOC is invisible. (For interpretation of the references to color in this figure legend, the reader is referred to the Web version of this article.)

then use 11 bins spaced by one order of magnitude in saturation mass concentration from 2 to −8 and use one additional overflow bin for all peaks with a volatility at 300K below −8.5 and calculate the concentration averaged mean mass of each bin. In this example case we also perform the same binning also for the dataset collected by the CIMS and PTR3 only. Fig. 6a shows the resulting VBS distributions at 300 K showing that especially in the lower O:C range, i.e. at nominal volatilities above −2, the sensitivity of the nitrate-CI decreases and additional peaks are identified by the PTR3 (Riva et al., 2019; D. Stolzenburg et al., 2018). When adjusting the VBS to the temperature of the experiment (Fig. 6b, using the Stolzenburg et al. (2018) temperature parametrization), we see that these additional contributions are also relevant down to the actual ELVOC range.

The VBS distribution (at 278 K, i.e. 5 °C) is then used as input for the dynamic growth model and Fig. 6c and d shows that we obtain a reasonable agreement between the modeled and measured GR using the DMA-train (D. Stolzenburg et al., 2017) and a conventional TSI nano-SMPS (Tröstl et al., 2015). Fig. 6c also demonstrates that the contribution of the PTR3 peaks is essential to catch the growth rate at larger sizes. Fig. 6d resolves the contributions of the individual bins to the growth rate following the procedure related to Eq. (18). That way we obtain an understanding which compounds are essential for nanoparticle growth under these experimental conditions. In the initial 1–2 nm range the ULVOC molecules still matter, but their contribution quickly falls off due to the non-negligible effect of vapor molecular size in their collisions. Afterwards, it is mainly ELVOC and LVOC compounds driving the growth, with an increasing contribution of LVOC compounds above 3–5 nm, the size range of the organic Kelvin-diameter (D. Stolzenburg et al., 2018). Overall, this example should demonstrate that the choice of ionization chemistry in OOM detection is crucial for such growth calculations, and it is especially the ELVOC and LVOC ranges which need to have good observational coverage. The highly selective (towards high O:C detection) nitrate-CI needs to be supported by other instruments if mass closure between gas- and particle-phase should be achieved.

3.3. Hyytiälä

Second we use a dataset recorded at the SMEAR II station in Hyytiälä, Finland (Hari & Kulmala, 2005), one of the best characterized

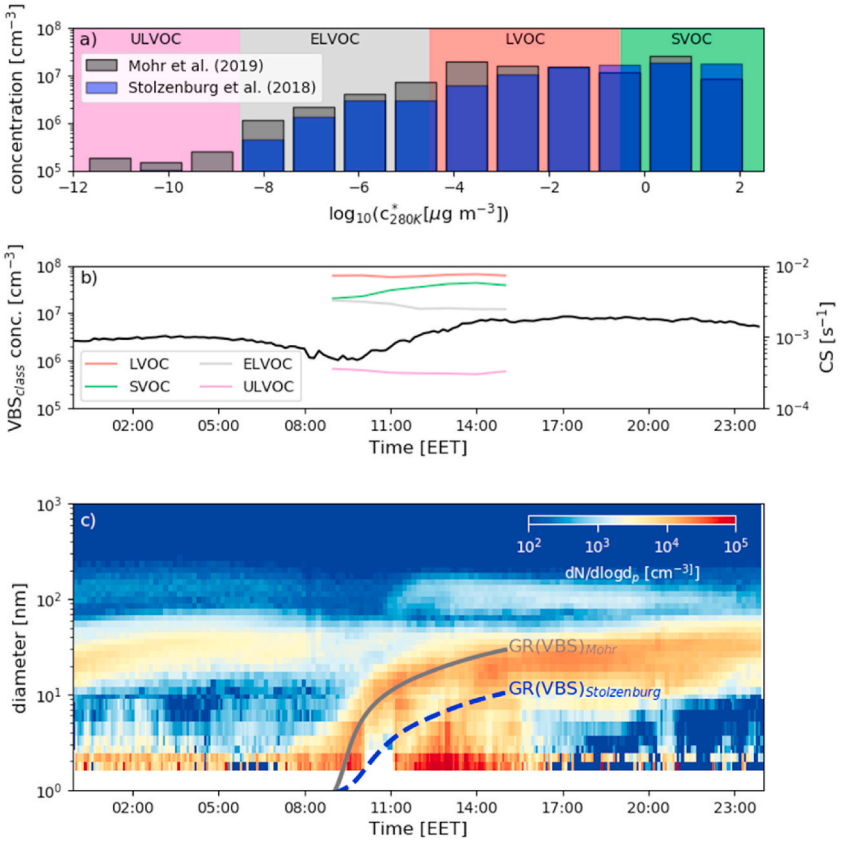

Fig. 7. VBS dynamic growth modelling for an ambient dataset recorded on the 7th of May 2020 in Hyytiälä, Finland. (a) shows the average VBS distribution at 280 K during the growth period for two volatility parametrizations, gray using Mohr et al. (2019) and blue using Stolzenburg et al. (2018). (b) shows the time-dependence of the four different volatility classes of interest and the condensation sink, illustrating their coupling and hence the necessity for a time-dependent growth modelling. (c) shows the measured particle size-distribution and two modelled growth trajectories, with the gray solid line using the Mohr et al. (2019) parametrization and the dashed blue line using the Stolzenburg et al. (2018) parametrization. (For interpretation of the references to color in this figure legend, the reader is referred to the Web version of this article.)

measurement sites for atmospheric NPF. Here, we do not have two complementary ionization chemistries available but use data from a nitrate–CI–APi-ToF only. Its limited sensitivity towards less oxygenated compounds will result in underestimated LVOC fractions at the T = 7 °C of the observations (Riva et al., 2019), possibly resulting in reduced growth rates >5 nm, similar to Tröstl et al. (2016). Moreover, in Hyytiälä also sulfuric acid and ammonia are expected to contribute to the particle growth, however their effect should be minor (Mohr et al., 2019).

We refer to model treating acid-base chemistry explicitly for the inclusion of sulfuric acid and ammonia (Yli-Juuti et al., 2013). Generally, the Hyytiälä dataset is characterized by larger uncertainties in the 2d-VBS relations as the OOMs will not only originate from dark α-pinene ozonolysis and their average functionalization is thus less precisely known compared to the well-controlled chamber experiments. Fig. 7a shows the average VBS over the growth period on the 7th of May 2020 and compares two different volatility parametrizations at the average temperature of the observation. The parametrization of Mohr et al. (2019) clearly results in more ULVOC and ELVOC compounds compared to the parametrization of Stolzenburg et al. (2018), mainly due to the reduced oxygen effect for the covalently bound dimers (all compounds with $n_C > 10$) in Stolzenburg et al. (2018). However also in the LVOC range the Mohr et al. (2019) parametrization yields slightly higher yields due to the decreased volatility at lower O:C assuming the hydroperoxides only start to contribute significantly at higher oxidation states in the autoxidation process.

Furthermore, in the example case, we use time-dependent data of measured OOMs concentrations as sources and sinks vary more significantly in this ambient setting were the sampled air mass is not necessarily constant and hence condensation patterns might change due to changing vapor concentrations. This can be seen in Fig. 7b, where the concentrations of the different volatility groups are shown during the growth period together with the condensation sink. Apparently, the increasing sink due to the newly formed particles also significantly decreases the steady-state ULVOC and ELVOC concentrations (and to some extent also the LVOC concentrations, please note the log-scale), while SVOC concentrations still rise. Note that, we use time-dependent bin concentrations, but do not fill the VBS at every time-step neglecting the fact that also temperature might change to some, albeit minor, extent, which would result in a different VBS for each time-step.

The time-dependent growth modeling is then transformed into a diameter-time growth trajectory which is shown in Fig. 7c on top of the measured particle-size distribution using a DMA-train (D. Stolzenburg et al., 2017) and a twin-DMPS (Aalto et al., 2001). As we can see, it is mostly the lower ULVOC and especially ELVOC concentrations which result in slower initial growth using the parametrization by Stolzenburg et al. (2018), while the later growth is described similarly by both volatility parametrizations (similar slope of the trajectories). Surprisingly, the results from the Mohr et al. (2019) parametrization nicely catch the growing mode, despite the fact that LVOC concentrations might still be underestimated. Altogether, as we can see from this example, the dynamic VBS growth modeling heavily relies on the underlying parametrizations and the instrumentation used for gas-phase measurement; this should always be taken into consideration when the method is used.

4. Conclusion

In this tutorial we reviewed the basics of the volatility basis set for describing the phase-transition process of OOMs. We clarified the basic concepts of the VBS and illustrated its origin in partitioning theory. We then showed how to construct a 2-dimensional VBS with the degree of oxygenation as the second axis and showed how a VBS is filled from gas- or particle phase composition measurements and then transformed upon temperature change. Using the basic equations of mass transfer, we developed a monodisperse particle growth model, which can use a VBS distribution as input in order to model the resulting growth of a monodisperse particle population, which can be used as a single-particle growth rate estimate for organic aerosol growth in ambient settings.

We showed its application to two datasets, one from a well-controlled chamber experiment and one from ambient measurements, illustrating that special care has to be taken when gas-phase measurements are transformed into a VBS. We showed that substantial error can be introduced by an incomplete range of sensitivity of OOMs. Overall, the method crucially depends on good volatility estimates and quantification of the gas-phase compounds, where we still lack suitable calibration substances. Moreover, the model itself is a pure monodisperse growth model and considers neither size-distribution dynamics such as self- and extramodal-coagulation (M. R. Stolzenburg et al., 2005) nor diffusion-driven growth (Olenius et al., 2018).

Apart from these limitations this method has shown to be useful in describing organic growth in both chamber and ambient settings and is a straightforward way to estimate the contribution of organics to initial growth accounting for the wide-range of volatility observed in atmospheric OOMs. This tutorial provides the necessary basics for performing such calculations in the future and together with the openly available python package should foster its usage.

About this article

This article is an Editor-Invited Tutorial Article. Tutorial articles, established to commemorate the 50th Anniversary of the Journal of Aerosol Science in 2020, are intended to serve as educational resources for the aerosol research community on state-of-the-art experimental, theoretical, and numerical techniques in aerosol science.

Data availability

Current version of the code can be found on https://version.helsinki.fi/atm-public/vbsgrowth, the version upon acceptance including the analysis input data will achieved under https://doi.org/10.23729/d213ae5d-fa3c-4b3e-b18c-7357c8f089ed.

Declaration of competing interest

The authors declare that they have no known competing financial interests or personal relationships that could have appeared to influence the work reported in this paper.

Acknowledgements

We acknowledge Wayne Chuang for his contribution to the first dynamic VBS growth modelling tool, which was the basis for the code developed here. We also thank Nina Sarnela, Martin Heinritzi and Mario Simon for the mass spectrometric analysis of the two presented example cases and acknowledge Loic Gonzales-Carracedo for the deployment of the DMA-train in Hyytiälä. This research has received funding from the European Union's Horizon 2020 research and innovation programme under the Marie Sklodowska-Curie grant agreement no. 895875 ("NPF-PANDA"). We acknowledge the funding from the US National Science Foundation AGS2132089.

References

Aalto, P., Hämeri, K., Becker, E., Weber, R., Salm, J., Mäkelä, J. M., et al. (2001). Physical characterization of aerosol particles during nucleation events. *Tellus B: Chemical and Physical Meteorology, 53*(4), 344–358. https://doi.org/10.3402/tellusb.v53i4.17127

Aiken, A. C., DeCarlo, P. F., Kroll, J. H., Worsnop, D. R., Huffman, J. A., Docherty, K. S., et al. (2008). O/C and OM/OC ratios of primary, secondary, and ambient organic aerosols with high-resolution time-of-flight aerosol mass spectrometry. *Environmental Science & Technology, 42*(12), 4478–4485. https://doi.org/10.1021/es703009q

Bannan, T. J., Le Breton, M., Priestley, M., Worrall, S. D., Bacak, A., Marsden, N. A., et al. (2019). A method for extracting calibrated volatility information from the FIGAERO-HR-ToF-CIMS and its experimental application. *Atmospheric Measurement Techniques, 12*(3), 1429–1439. https://doi.org/10.5194/amt-12-1429-2019

Bianchi, F., Kurtén, T., Riva, M., Mohr, C., Rissanen, M. P., Roldin, P., et al. (2019). Highly oxygenated organic molecules (HOM) from gas-phase Autoxidation Involving peroxy radicals: A key contributor to atmospheric aerosol. *Chemistry Review, 119*(6), 3472–3509. https://doi.org/10.1021/acs.chemrev.8b00395

Bianchi, F., Tröstl, J., Junninen, H., Frege, C., Henne, S., Hoyle, C. R., et al. (2016). New particle formation in the free troposphere: A question of chemistry and timing. *Science, 352*(6289), 1109–1112. https://doi.org/10.1126/science.aad5456

Breitenlechner, M., Fischer, L., Hainer, M., Heinritzi, M., Curtius, J., & Hansel, A. (2017). PTR3: An instrument for studying the lifecycle of reactive organic carbon in the atmosphere. *Analytical Chemistry, 89*(11), 5824–5831. https://doi.org/10.1021/acs.analchem.6b05110

Chuang, W. K., & Donahue, N. M. (2016). A two-dimensional volatility basis set – Part 3: Prognostic modeling and NO$_x$ dependence. *Atmospheric Chemistry and Physics, 16*(1), 123–134. https://doi.org/10.5194/acp-16-123-2016

Chuang, W. K., & Donahue, N. M. (2017). Dynamic consideration of smog chamber experiments. *Atmospheric Chemistry and Physics, 17*(16), 10019–10036. https://doi.org/10.5194/acp-17-10019-2017

Daellenbach, K. R., Uzu, G., Jiang, J., Cassagnes, L.-E., Leni, Z., Vlachou, A., et al. (2020). Sources of particulate-matter air pollution and its oxidative potential in Europe. *Nature, 587*(7834), 414–419. https://doi.org/10.1038/s41586-020-2902-8

Donahue, N. M., Epstein, S. A., Pandis, S. N., & Robinson, A. L. (2011). A two-dimensional volatility basis set: 1. Organic-aerosol mixing thermodynamics. *Atmospheric Chemistry and Physics, 11*(7), 3303–3318. https://doi.org/10.5194/acp-11-3303-2011

Donahue, N. M., Kroll, J. H., Pandis, S. N., & Robinson, A. L. (2012). A two-dimensional volatility basis set – Part 2: Diagnostics of organic-aerosol evolution. *Atmospheric Chemistry and Physics, 12*(2), 615–634. https://doi.org/10.5194/acp-12-615-2012

Donahue, N. M., Robinson, A. L., & Pandis, S. N. (2009). Atmospheric organic particulate matter: From smoke to secondary organic aerosol. *Atmospheric Environment, 43*(1), 94–106. https://doi.org/10.1016/j.atmosenv.2008.09.055

Donahue, N. M., Robinson, A. L., Stanier, C. O., & Pandis, S. N. (2006). Coupled partitioning, dilution, and chemical aging of semivolatile organics. *Environmental Science & Technology, 40*(8), 2635–2643. https://doi.org/10.1021/es052297c

Donahue, N. M., Trump, E. R., Pierce, J. R., & Riipinen, I. (2011). Theoretical constraints on pure vapor-pressure driven condensation of organics to ultrafine particles. *Geophysical Research Letters, 38*(16). https://doi.org/10.1029/2011GL048115. n/a–n/a.

Ehn, M., Thornton, J. A., Kleist, E., Sipila, M., Junninen, H., Pullinen, I., et al. (2014). A large source of low-volatility secondary organic aerosol. *Nature, 506*, 476–479. https://doi.org/10.1038/nature13032

Epstein, S. A., Riipinen, I., & Donahue, N. M. (2010). A semiempirical correlation between enthalpy of vaporization and saturation concentration for organic aerosol. *Environmental Science & Technology, 44*(2), 743–748. https://doi.org/10.1021/es902497z

Fuchs, N. A., & Sutugin, A. G. (1971). High dispersed aerosols. In G. M. Hidy, & J. R. Brock (Eds.), *Topics in current aerosol research (Part 2)* (pp. 1–200). Pergamon.

Goldstein, A. H., & Galbally, I. E. (2007). Known and unexplored organic constituents in the Earth's atmosphere. *Environmental Science & Technology, 41*(5), 1514–1521. https://doi.org/10.1021/es072476p

Gordon, H., Kirkby, J., Baltensperger, U., Bianchi, F., Breitenlechner, M., Curtius, J., et al. (2017). Causes and importance of new particle formation in the present-day and preindustrial atmospheres. *Journal of Geophysical Research: Atmospheres, 122*. https://doi.org/10.1002/2017JD026844

Hallquist, M., Wenger, J. C., Baltensperger, U., Rudich, Y., Simpson, D., Claeys, M., et al. (2009). The formation, properties and impact of secondary organic aerosol: Current and emerging issues. *Atmospheric Chemistry and Physics, 9*(14), 5155–5236. https://doi.org/10.5194/acp-9-5155-2009

Hari, P., & Kulmala, M. (2005). Station for measuring ecosystem–atmosphere relations (SMEAR II). *Boreal Environment Research, 10*, 315–322.

Jimenez, J. L., Canagaratna, M. R., Donahue, N. M., Prevot, A. S. H., Zhang, Q., Kroll, J. H., et al. (2009). Evolution of organic aerosols in the atmosphere. *Science, 326*(5959), 1525–1529. https://doi.org/10.1126/science.1180353

Jokinen, T., Sipilä, M., Junninen, H., Ehn, M., Lönn, G., Hakala, J., et al. (2012). Atmospheric sulphuric acid and neutral cluster measurements using CI-APi-TOF. *Atmospheric Chemistry and Physics, 12*(9), 4117–4125. https://doi.org/10.5194/acp-12-4117-2012

Kirkby, J., Curtius, J., Almeida, J., Dunne, E., Duplissy, J., Ehrhart, S., et al. (2011). Role of sulphuric acid, ammonia and galactic cosmic rays in atmospheric aerosol nucleation. *Nature, 476*, 429–433. https://doi.org/10.1038/nature10343

Kirkby, J., Duplissy, J., Sengupta, K., Frege, C., Gordon, H., Williamson, C., et al. (2016). Ion-induced nucleation of pure biogenic particles. *Nature, 533*, 521–526. https://doi.org/10.1038/nature17953

Krieger, U. K., Siegrist, F., Marcolli, C., Emanuelsson, E. U., Gøbel, F. M., Bilde, M., et al. (2018). A reference data set for validating vapor pressure measurement techniques: Homologous series of polyethylene glycols. *Atmospheric Measurement Techniques, 11*(1), 49–63. https://doi.org/10.5194/amt-11-49-2018

Kulmala, M., Kontkanen, J., Junninen, H., Lehtipalo, K., Manninen, H. E., Nieminen, T., et al. (2013). Direct observations of atmospheric aerosol nucleation. *Science, 339*(6122), 943–946. https://doi.org/10.1126/science.1227385

La, Y. S., Camredon, M., Ziemann, P. J., Valorso, R., Matsunaga, A., Lannuque, V., et al. (2016). Impact of chamber wall loss of gaseous organic compounds on secondary organic aerosol formation: Explicit modeling of \hack{\newline}SOA formation from alkane and alkene oxidation. *Atmospheric Chemistry and Physics, 16*(3), 1417–1431. https://doi.org/10.5194/acp-16-1417-2016

Lane, T. E., Donahue, N. M., & Pandis, S. N. (2008). Simulating secondary organic aerosol formation using the volatility basis-set approach in a chemical transport model. *Atmospheric Environment, 42*(32), 7439–7451. https://doi.org/10.1016/j.atmosenv.2008.06.026

Lee, B. H., Lopez-Hilfiker, F. D., Mohr, C., Kurtén, T., Worsnop, D. R., & Thornton, J. A. (2014). An iodide-adduct high-resolution time-of-flight chemical-ionization mass spectrometer: Application to atmospheric inorganic and organic compounds. *Environmental Science & Technology, 48*(11), 6309–6317. https://doi.org/10.1021/es500362a

Lehtinen, K. E. J., & Kulmala, M. (2003). A model for particle formation and growth in the atmosphere with molecular resolution in size. *Atmospheric Chemistry and Physics, 3*(1), 251–257. https://doi.org/10.5194/acp-3-251-2003

Lopez-Hilfiker, F. D., Mohr, C., Ehn, M., Rubach, F., Kleist, E., Wildt, J., et al. (2014). A novel method for online analysis of gas and particle composition: Description and evaluation of a {F}ilter {I}nlet for {G}ases and {AERO}sols ({FIGAERO}). *Atmospheric Measurement Techniques, 7*(4), 983–1001. https://doi.org/10.5194/amt-7-983-2014

IPCC. (2021). In V. Masson-Delmotte, P. Zhai, A. Pirani, S. L. Connors, C. Péan, S. Berger, et al. (Eds.), *In pressClimate change 2021: The physical science basis. Contribution of working group I to the sixth assessment report of the intergovernmental panel on climate change*. Cambridge University Press.

Mohr, C., Thornton, J. A., Heitto, A., Lopez-Hilfiker, F. D., Lutz, A., Riipinen, I., et al. (2019). Molecular identification of organic vapors driving atmospheric nanoparticle growth. *Nature Communications, 10*(1), 4442. https://doi.org/10.1038/s41467-019-12473-2

Nieminen, T., Lehtinen, K. E. J., & Kulmala, M. (2010). Sub-10 nm particle growth by vapor condensation – effects of vapor molecule size and particle thermal speed. *Atmospheric Chemistry and Physics, 10*(20), 9773–9779. https://doi.org/10.5194/acp-10-9773-2010

Nie, W., Yan, C., Huang, D. D., Wang, Z., Liu, Y., Qiao, X., et al. (2022). Secondary organic aerosol formed by condensing anthropogenic vapours over China's megacities. *Nature Geoscience, 15*, 255–261. https://doi.org/10.1038/s41561-022-00922-5

Odum, J. R., Hoffmann, T., Bowman, F., Collins, D., Flagan, R. C., & Seinfeld, J. H. (1996). Gas/particle partitioning and secondary organic aerosol yields. *Environmental Science & Technology, 30*(8), 2580–2585. https://doi.org/10.1021/es950943+

Olenius, T., Pichelstorfer, L., Stolzenburg, D., Winkler, P. M., Lehtinen, K. E. J., & Riipinen, I. (2018). Robust metric for quantifying the importance of stochastic effects on nanoparticle growth. *Scientific Reports, 8*(1), Article 14160. https://doi.org/10.1038/s41598-018-32610-z

Ouyang, H., Gopalakrishnan, R., & Hogan, C. J. (2012). Nanoparticle collisions in the gas phase in the presence of singular contact potentials. *Journal of Chemical Physics, 137*(6), Article 64316. https://doi.org/10.1063/1.4742064

Pankow, J. F. (1994a). An absorption model of gas/particle partitioning of organic compounds in the atmosphere. *Atmospheric Environment, 28*(2), 185–188. https://doi.org/10.1016/1352-2310(94)90093-0

Pankow, J. F. (1994b). An absorption model of the gas/aerosol partitioning involved in the formation of secondary organic aerosol. *Atmospheric Environment, 28*(2), 189–193. https://doi.org/10.1016/1352-2310(94)90094-9

Pankow, J. F., & Asher, W. E. (2008). SIMPOL.1: A simple group contribution method for predicting vapor pressures and enthalpies of vaporization of multifunctional organic compounds. *Atmospheric Chemistry and Physics, 8*, 2773–2796. https://doi.org/10.5194/acp-8-2773-2008

Pierce, J. R., Riipinen, I., Kulmala, M., Ehn, M., Petäjä, T., Junninen, H., et al. (2011). Quantification of the volatility of secondary organic compounds in ultrafine particles during nucleation events. *Atmospheric Chemistry and Physics, 11*(17), 9019–9036. https://doi.org/10.5194/acp-11-9019-2011

Presto, A. A., & Donahue, N. M. (2006). Investigation of α-pinene + ozone secondary organic aerosol formation at low total aerosol mass. *Environmental Science & Technology, 40*(11), 3536–3543. https://doi.org/10.1021/es052203z

Riipinen, I., Pierce, J. R., Yli-Juuti, T., Nieminen, T., Häkkinen, S., Ehn, M., et al. (2011). Organic condensation: A vital link connecting aerosol formation to cloud condensation nuclei (CCN) concentrations. *Atmospheric Chemistry and Physics, 11*(8), 3865–3878. https://doi.org/10.5194/acp-11-3865-2011

Riva, M., Rantala, P., Krechmer, J. E., Peräkylä, O., Zhang, Y., Heikkinen, L., et al. (2019). Evaluating the performance of five different chemical ionization techniques for detecting gaseous oxygenated organic species. *Atmospheric Measurement Techniques, 12*(4), 2403–2421. https://doi.org/10.5194/amt-12-2403-2019

Seinfeld, J., & Pandis, S. (2016). *Atmospheric chemistry and Physics: From air pollution to climate change* (3rd ed.). Wiley.

Simon, M., Dada, L., Heinritzi, M., Scholz, W., Stolzenburg, D., Fischer, L., et al. (2020). Molecular understanding of new-particle formation from alpha-pinene between -50 and +25 °C. *Atmospheric Chemistry and Physics, 20*(15), 9183–9207. https://doi.org/10.5194/acp-20-9183-2020

Spracklen, D. V., Jimenez, J. L., Carslaw, K. S., Worsnop, D. R., Evans, M. J., Mann, G. W., et al. (2011). Aerosol mass spectrometer constraint on the global secondary organic aerosol budget. *Atmospheric Chemistry and Physics, 11*(23), 12109–12136. https://doi.org/10.5194/acp-11-12109-2011

Stolzenburg, D., Fischer, L., Vogel, A. L., Heinritzi, M., Schervish, M., Simon, M., et al. (2018). Rapid growth of organic aerosol nanoparticles over a wide tropospheric temperature range. *P. Nat. Acad. Sci. USA, 115*(37), 9122–9127. https://doi.org/10.1073/pnas.1807604115

Stolzenburg, M. R., McMurry, P. H., Sakurai, H., Smith, J. N., Mauldin, R. L., III, Eisele, F. L., et al. (2005). Growth rates of freshly nucleated atmospheric particles in Atlanta. *Journal of Geophysical Research: Atmospheres, 110*(D22). https://doi.org/10.1029/2005JD005935

Stolzenburg, D., Simon, M., Ranjithkumar, A., Kürten, A., Lehtipalo, K., Gordon, H., et al. (2020). Enhanced growth rate of atmospheric particles from sulfuric acid. *Atmospheric Chemistry and Physics, 20*(12), 7359–7372. https://doi.org/10.5194/acp-20-7359-2020

Stolzenburg, D., Steiner, G., & Winkler, P. M. (2017). A DMA-train for precision measurement of sub-10 nm aerosol dynamics. *Atmospheric Measurement Techniques, 10*(4), 1639–1651. https://doi.org/10.5194/amt-10-1639-2017

Tröstl, J., Chuang, W. K., Gordon, H., Heinritzi, M., Yan, C., Molteni, U., et al. (2016). The role of low-volatility organic compounds in initial particle growth in the atmosphere. *Nature, 533*, 527–531. https://doi.org/10.1038/nature18271

Tröstl, J., Tritscher, T., Bischof, O. F., Horn, H.-G., Krinke, T., Baltensperger, U., et al. (2015). Fast and precise measurement in the sub-20 nm size range using a Scanning Mobility Particle Sizer. *Journal of Aerosol Science, 87*, 75–87. https://doi.org/10.1016/j.jaerosci.2015.04.001

Tsigaridis, K., Daskalakis, N., Kanakidou, M., Adams, P. J., Artaxo, P., Bahadur, R., et al. (2014). The AeroCom evaluation and intercomparison of organic aerosol in global models. *Atmospheric Chemistry and Physics, 14*(19), 10845–10895. https://doi.org/10.5194/acp-14-10845-2014

Wang, M., Chen, D., Xiao, M., Ye, Q., Stolzenburg, D., Hofbauer, V., et al. (2020). Photo-oxidation of aromatic hydrocarbons produces low-volatility organic compounds. *Environmental Science & Technology, 54*(13). https://doi.org/10.1021/acs.est.0c02100

Yan, C., Nie, W., Vogel, A. L., Dada, L., Lehtipalo, K., Stolzenburg, D., et al. (2020). Size-dependent influence of NOx on the growth rates of organic aerosol particles. *Science Advances, 6*(22), Article eaay4945. https://doi.org/10.1126/sciadv.aay4945

Ye, Q., Wang, M., Hofbauer, V., Stolzenburg, D., Chen, D., Schervish, M., et al. (2019). Molecular composition and volatility of nucleated particles from α-pinene oxidation between -50 °c and +25 °c. *Environmental Science & Technology, 53*(21). https://doi.org/10.1021/acs.est.9b03265

Yli-Juuti, T., Barsanti, K., Hildebrandt Ruiz, L., Kieloaho, A.-J., Makkonen, U., Petäjä, T., et al. (2013). Model for acid-base chemistry in nanoparticle growth (MABNAG). *Atmospheric Chemistry and Physics, 13*(24), 12507–12524. https://doi.org/10.5194/acp-13-12507-2013

Ylisirniö, A., Barreira, L. M. F., Pullinen, I., Buchholz, A., Jayne, J., Krechmer, J. E., et al. (2021). On the calibration of FIGAERO-ToF-CIMS: Importance and impact of calibrant delivery for the particle-phase calibration. *Atmospheric Measurement Techniques, 14*(1), 355–367. https://doi.org/10.5194/amt-14-355-2021

Zhang, X., Cappa, C. D., Jathar, S. H., McVay, R. C., Ensberg, J. J., Kleeman, M. J., et al. (2014). Influence of vapor wall loss in laboratory chambers on yields of secondary organic aerosol. *P. Nat. Acad. Sci. USA, 111*(16), 5802–5807. https://doi.org/10.1073/pnas.1404727111

Zhang, X., Pandis, S. N., & Seinfeld, J. H. (2012). Diffusion-limited versus quasi-equilibrium aerosol growth. *Aerosol Science & Technology, 46*(8), 874–885. https://doi.org/10.1080/02786826.2012.679344

Zhao, D., Schmitt, S. H., Wang, M., Acir, I.-H., Tillmann, R., Tan, Z., et al. (2018). Effects of NOx and SO2 on the secondary organic aerosol formation from photooxidation of alpha-pinene and limonene. *Atmospheric Chemistry and Physics, 18*(3), 1611–1628. https://doi.org/10.5194/acp-18-1611-2018

Dominik Stolzenburg is Marie-Curie Individual Fellowship funded Postdoctoral Researcher at the Institute for Atmospheric and Earth System Research of the University of Helsinki. He obtained his Ph.D. in Physics on nanoparticle growth measurements from the University of Vienna. His research focuses on nanoparticle growth processes and related measurement, analysis and modeling approaches.

Mingyi Wang is a postdoctoral fellow in Chemical Engineering at the California Institute of Technology. He received a Ph.D. in Chemistry from Carnegie Mellon University. His research focuses on oxidative chemistry and microphysics of atmospheric new particle formation via ambient measurement, laboratory experiment, and theory.

Meredith Schervish received a BA in chemistry and mathematics at The College of Wooster and a PhD in chemistry from Carnegie Mellon University. She is currently a postdoctoral scholar at the University of California, Irvine where she studies multiphase chemistry and the kinetics and thermodynamics surrounding gas-phase uptake into aerosol particles.

Neil Donahue is an atmospheric chemist at Carnegie Mellon University, where he is the Lord University Professor of Chemistry in the departments of Chemistry, Chemical Engineering and Engineering and Public Policy. He received an AB in Physics from Brown University and a PhD in Meteorology from MIT.